

# Modeling of Densification Kinetics during Electro-Pulse Consolidation of Titanium Powder

Olha Syzonenko, Mykola Prystash, Andrii Torpakov, Tetiana Makrukha

Institute of Pulse Processes and Technologies of NAS of Ukraine, Bohoyavlenskyi ave., 43-A, 54018, Mykolaiv, Ukraine  
olgasyzonenko43@gmail.com

**Abstract** This study presents a theoretical investigation of the densification kinetics of titanium powder during electro-pulse consolidation. A mathematical model was developed to analyze the influence of electrical current parameters in different sintering regimes – direct current (DC), alternating current (AC), pulsed current, and their superposition – on the thermophysical processes governing sintering. The heating rates and the evolution of relative density were calculated for different applied pressing pressures. The results show that the superposition of currents is the most energy-efficient regime. This regime enables the material to reach a relative density above 99% within a minimal processing time. The effect is attributed to the combined action of intense Joule heating and the electroplastic effect.

**KEYWORDS:** TITANIUM POWDER, ELECTRO-PULSE CONSOLIDATION, DENSIFICATION KINETICS, JOULE HEATING, CURRENT SUPERPOSITION, SPARK PLASMA SINTERING.

## 1. Introduction

The production of high-density materials from refractory metals, particularly titanium, while preserving their microstructure remains an important challenge in materials science. Conventional sintering methods require prolonged thermal exposure, which promotes grain growth and leads to degradation of physical and mechanical properties.

The use of Electric Current Assisted Sintering (ECAS) technologies is a promising approach to address these issues. These methods provide rapid powder densification due to intensive Joule heating and electroplastic effects.

The modern market offers various types of equipment for electroconsolidation. Spark plasma sintering (SPS) is the most widely used ECAS technique. It employs pulsed current (typically ~1 kHz). This approach is implemented in systems such as the Dr. Sinter SPS series (SPS Syntex Inc.) [1] and HP D systems (FCT Systeme GmbH) [2]. For studies focused on the influence of alternating current (AC), direct current (DC), and their combinations, physical simulation systems such as the Gleeble 3800 [3] are often used, as they allow flexible control of the current waveform. Some experimental setups, for example the Gefest-10 [4], enable the application of current superposition to achieve a synergistic densification effect.

Despite the availability of different equipment, direct experimental comparison of the efficiency of various current regimes (DC, AC, pulsed current, and superposition) for the same material is challenging. Differences in chamber design, thermal units, and tooling geometry in industrial systems prevent the creation of identical processing conditions required for rigorous analysis.

To address this limitation, a theoretical modeling approach to densification kinetics was adopted. This method eliminates the influence of equipment-specific design factors. Titanium powder was selected as the model material because its relatively high electrical resistivity makes it well suited for the analysis of electrothermal processes.

The aim of this study is to theoretically investigate and compare the densification kinetics of titanium powder under different current regimes and applied pressures in order to determine energy-efficient consolidation conditions.

## 2. Methodology

This study is based on a supervised machine learning methodology. The general scheme of the model represents a powder compact placed inside a die between two punches. To ensure the adequacy and physical consistency of the model, several key assumptions were adopted [6]:

1. The temperature field inside the sample is assumed to be spatially uniform at any given time. This assumption is justified for small specimens and high heating rates typical of the process.

2. The electrical resistance is calculated for the entire specimen volume and treated as a single equivalent resistive element.

3. Heat losses to the environment through the die and punches are neglected.

4. The densification kinetics are described using phenomenological equations. The model parameters are calibrated to qualitatively reproduce experimentally observed trends rather than to simulate micromechanical processes at the level of individual particle contacts.

### Mathematical Description of the Model

The model is based on a system of coupled differential and algebraic equations that describe heat generation, thermal balance, and the kinetics of structural evolution in the powder compact.

### Electrophysical Submodel and Calculation of Joule Heating

The primary energy source during the process is Joule heat generation. The instantaneous power of heat release,  $Q$ , W, is calculated according to the Joule–Lenz law [5]:

$$Q = I_{eff}^2 \cdot R(t), \quad (1)$$

where  $I_{eff}$  is the effective (root mean square, RMS) current (A), and  $R(t)$  is the instantaneous electrical resistance of the sample ( $\Omega$ ).

An important feature of the proposed model is the inclusion of the dynamic change in the specimen height,  $h_{current}(t)$ , during densification. This variation is calculated according to the law of mass conservation:

$$h_{current}(t) = h_{initial} \cdot \frac{\rho_{rel,initial}}{\rho_{rel}(t)}. \quad (2)$$

The instantaneous electrical resistance, in turn, is a function of the specimen geometry and its effective electrical conductivity,  $\sigma_{eff}$ :

$$R(t) = \frac{h_{current}(t)}{\sigma_{eff}(t) \cdot A_{sample}}, \quad (3)$$

where

$$A_{sample} = \pi \left( \frac{d_{sample}}{2} \right)^2, \quad (4)$$

The effective electrical conductivity,  $\sigma_{eff}$ , of the powder compact is approximated by a linear relationship between the electrical conductivity of the fully dense material  $\sigma_{Ti}$  and the current relative density  $\rho_{rel}(t)$ .

$$\sigma_{eff}(t) = \sigma_{Fe} \cdot \rho_{rel}(t). \quad (5)$$

### Evaluation of the Effective Current

A key aspect of the electrophysical submodel is the accurate calculation of the effective current,  $I_{eff}$ , for different signal types

(see Figure 1), since the RMS value determines the average power released over an oscillation period.

The model considers four main types of current namely direct current (DC), sinusoidal alternating current at 50 Hz (AC), pulsed current (~1 kHz), and a superposition of direct and pulsed current at ~50 kHz, characteristic to the Gefest-10 system.

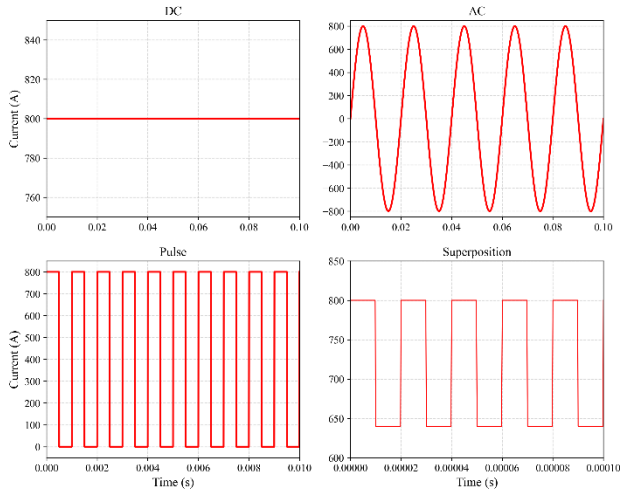


**Figure 1:** Considered current waveforms

The effective current,  $I_{eff}$ , for different waveform types was calculated as follows [7]:

Direct current :

$$I_{eff}^2 = I_{DC}^2. \quad (6)$$

Alternating sinusoidal current:

$$I_{eff}^2 = \left(\frac{I_{amp}}{\sqrt{2}}\right)^2 = \frac{I_{amp}^2}{2}. \quad (7)$$

Pulsed rectangular current with a duty cycle  $D = 0.5$ :

$$I_{eff}^2 = I_{amp}^2 \cdot D, \sigma_{eff}(t) = \sigma_{Fe} \cdot \rho_{rel}(t). \quad (8)$$

DC and AC superposition:

$$I_{eff}^2 = I_{DC,eff}^2 + I_{AC,eff}^2 = (0,8 \cdot I_{amp})^2 + \left(\frac{I_{amp}}{\sqrt{2}}\right)^2 = 0,66 \cdot I_{amp}^2. \quad (9)$$

The change in the average temperature of the sample,  $T$ , K, over time is described by the differential equation of thermal balance [8]:

$$m \cdot C_p \cdot \frac{dT}{dt} = Q_{eff}, \quad (10)$$

where  $m$  is the sample mass (kg),  $C_p$  is the specific heat capacity of the material (J/(kg·K)),  $T$  is the temperature (K), and  $Q_{eff}$  is the effective power of heat generation, W.

The averaged model does not account for the effects of increased contact resistance between particles and current concentration during the initial stages of sintering, which lead to significantly more intense heating. To compensate for this simplification, a phenomenological heating intensification factor,  $K_{heat}$ , is introduced. This factor increases the calculated Joule heating power during the heating stage ( $T < T_{target}$ ):

$$Q_{eff} = Q \cdot K_{heat}. \quad (11)$$

In this work, the value of this factor was taken as  $K_{heat} = 2.5$ .

To adequately describe the evolution of the relative density ( $\rho_{rel}$ ) and the microstructure of the sample over time, a phenomenological kinetic model based on the principle of superposition was considered. According to this principle, the overall densification rate is the sum of contributions from several simultaneously occurring mass transport mechanisms [9–10]:

Plastic deformation and creep – this mechanism dominates at relatively low temperatures and during the initial stages of densification. It is accounted for through a rate dependence on the current porosity ( $1 - \rho_{rel}$ ). The kinetic equation for this component is expressed as:

$$\left(\frac{d\rho_{rel}}{dt}\right)_{pl} = A_{pl} \cdot (1 - \rho_{rel}). \quad (12)$$

Here, the left-hand term represents the densification rate due to plastic mechanisms, and  $A_{pl}$  is an empirical coefficient characterizing the intensity of plastic flow and creep for the given material.

Thermally activated diffusion is the mechanism dominates at high temperatures and is responsible for the elimination of residual porosity during the intermediate and final stages of densification.

$$\left(\frac{d\rho_{rel}}{dt}\right)_{diff} = B_{diff} \cdot e^{-\frac{Q}{RT}} \cdot (1 - \rho_{rel}). \quad (13)$$

Here, the left-hand term represents the densification rate due to diffusion,  $B_{diff}$  is the pre-exponential factor,  $Q$  is the activation energy for diffusion of the material,  $R$  is the universal gas constant, and  $T$  is the absolute temperature.

The overall densification rate under standard conditions is the sum of the contributions from both mechanisms: plastic deformation/creep and thermally activated diffusion.

$$\begin{aligned} \left(\frac{d\rho_{rel}}{dt}\right)_{base} &= \left(\frac{d\rho_{rel}}{dt}\right)_{pl} + \left(\frac{d\rho_{rel}}{dt}\right)_{diff} = \\ &= A_{pl} \cdot (1 - \rho_{rel}) + B_{diff} \cdot e^{-\frac{Q}{RT}} \cdot (1 - \rho_{rel}). \end{aligned} \quad (14)$$

This base densification rate is further modified by the effects of pressure and athermal current phenomena. The influence of pressure ( $P$ ) is considered as a linear driving force normalized to a reference pressure,  $P_{ref}$ . Athermal effects (such as electromigration and electroplasticity) are accounted for using a dimensionless athermal activation factor,  $K_{athermal}$ , which takes the following values: 1 for DC, 1.05 for AC, 1.2 for pulsed current, and 1.3 for current superposition [11].

The final equation for the densification rate used in the model is obtained by multiplying the base rate by these two factors.

$$\frac{d\rho_{rel}}{dt} = \left(\frac{d\rho_{rel}}{dt}\right)_{base} \cdot K_{athermal} \cdot \left(\frac{P}{P_{ref}}\right). \quad (15)$$

By substituting the expression for the base densification rate, the final equation is obtained, which incorporates all relevant physical effects: plastic deformation and creep, thermally activated diffusion, applied pressure, and athermal current effects.

$$\begin{aligned} \frac{d\rho_{rel}}{dt} &= \left(A_{pl} \cdot (1 - \rho_{rel}) + B_{diff} \cdot e^{-\frac{Q}{RT}} \cdot (1 - \rho_{rel})\right) \cdot K_{athermal} \cdot \left(\frac{P}{P_{ref}}\right). \end{aligned} \quad (16)$$

The developed system of coupled differential equations is solved numerically using the explicit Euler method with a constant integration step of  $\Delta t = 0.1$  s.

The following constants [12] and initial conditions were used in the calculations:

Table 1. Initial conditions of the model

Parameter	Symbol	Value	Unit
Titanium density	$\rho_{Ti}$	4500	kg/m <sup>3</sup>
Titanium specific heat	$C_{p,Ti}$	523	J/(kg·K)
Titanium electrical conductivity	$\sigma_{Ti}$	$2.38 \cdot 10^6$	S/m
Diffusion activation energy (Ti)	$Q$	$1.53 \cdot 10^5$	J/mol
Sample diameter	$d_{sample}$	0.01	m
Sample height	$h_{sample}$	0.01	m
Initial relative density	$\rho_{rel,0}$	0.6	—
Initial temperature	$T_0$	293.15	K
Target temperature (Ti)	$T_{target}$	1607.55	K
Integration step	$\Delta t$	0.1	s
Maximum simulation time	$t_{max}$	60	s
Plasticity coefficient	$A_{pl}$	$8.00 \cdot 10^{-5}$	s <sup>-1</sup>
Diffusion coefficient	$B_{diff}$	$8.00 \cdot 10^4$	s <sup>-1</sup>

For quantitative evaluation and comparison of the efficiency of different consolidation modes, a scatter plot was constructed showing "Total Energy Consumption versus Final Relative Density" [13–15].

The entire computational framework was implemented in the Python programming language using its standard scientific and engineering libraries.

### 3. Results and discussion

The simulations were performed by varying the current intensity at 400, 600, and 800 A, and the applied pressing pressure at 20, 35, and 50 MPa. The temperature regime was defined as reaching approximately  $0.8 \cdot T_{melting} \approx 1300$  °C, followed by holding at this temperature until the maximum simulation time,  $t_{max}$ , was reached.

Based on the analysis of the obtained data, the heating rates for each consolidation regime were calculated (see Figure 2). At a current of 400 A, the heating rate was approximately 20 °C/s, regardless of the consolidation method. This is explained by insufficient power to reveal differences in thermal behavior at this energy level.

As the current increases, clear differentiation in heating efficiency is observed. At 600 A, the heating rate for samples processed with AC and pulsed current rises to about 30 °C/s, for the current superposition it reaches about 40 °C/s, while for DC it reaches approximately 60 °C/s. The most pronounced differences occur at 800 A: for AC and pulsed current, the heating rate increases to around 50 °C/s, for the current superposition to 70 °C/s, and for DC it reaches a maximum of approximately 120 °C/s.

This significant advantage of DC is attributed to the continuous generation of Joule heat, in contrast to AC or pulsed currents, where the effective power is reduced due to periodic zero crossings or pulse gaps. It is also noteworthy that the pressing pressure had little effect on the heating rate, indicating that volumetric heat generation dominates over contact resistance within the studied parameter range.

The presented densification curves for consolidation under direct current (see Figure 3) illustrate the nonlinear evolution of relative density, which can be divided into three characteristic stages:

1. An initial particle rearrangement stage with minimal density increase.

2. A stage of intensive plastic deformation and creep, where the densification rate reaches its maximum.

3. A final asymptotic stage corresponding to the closure of isolated pores.

At the maximum load (50 MPa) and a current of 800 A, the model predicts that the relative density reaches 0.99 by the 60th second of the process. In contrast, at 400 A and 20 MPa, the consolidation process is significantly prolonged.

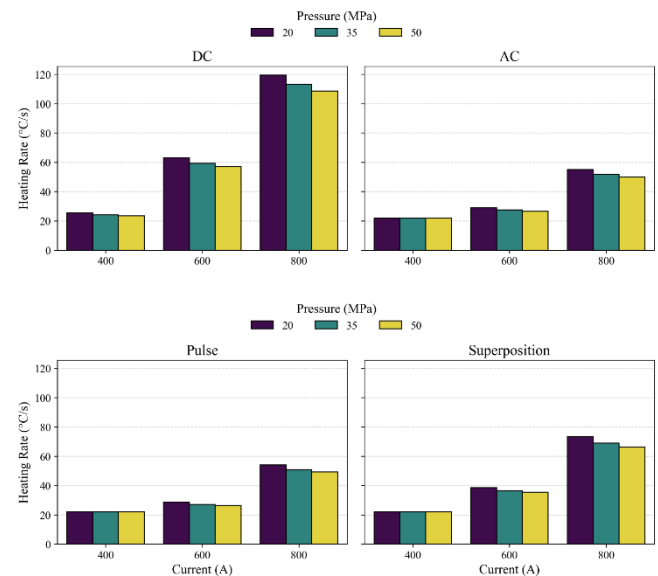


Figure 2: Comparative graphs of average heating rates

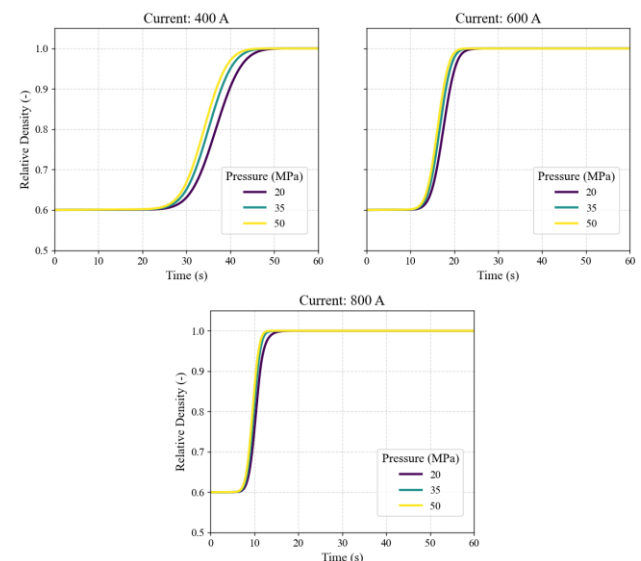
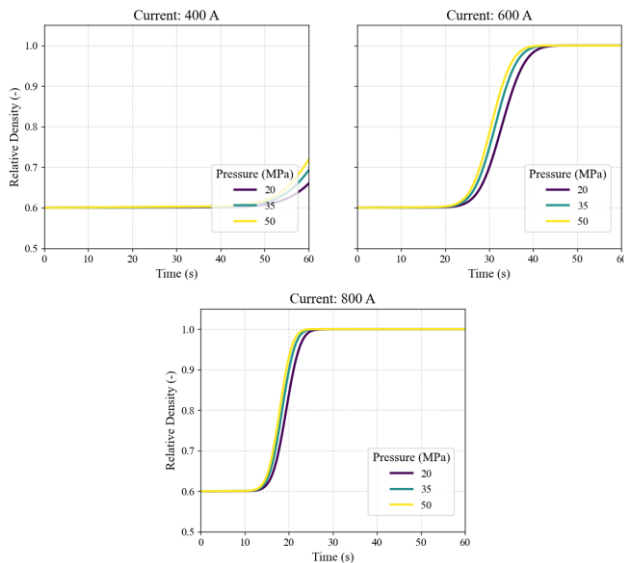


Figure 3: Evolution of the relative density of titanium powder during heating with direct current

The densification curves for alternating current (see Figure 4) show a delayed onset of intensive shrinkage compared to direct current of the same amplitude. However, due to the inclusion of the athermal activation factor, the densification rate during the active compaction stage is higher, allowing the relative density to reach 0.98–0.99 at 50 MPa. This indicates that the influence of the alternating field on the crystal lattice promotes more efficient stress relaxation.

Simulation results (see Figure 5) show that the pulsed current regime provides one of the fastest densification dynamics among the single-mode currents considered. The relative density curves exhibit a steep slope during the active sintering stage, which is

explained by the action of mechanisms such as surface oxide film removal and intensified mass transport under pulsed fields. This allows achieving a relative density of 0.99 in a shorter time than with direct current.



**Figure 4:** Evolution of the relative density of titanium powder during heating with alternating current

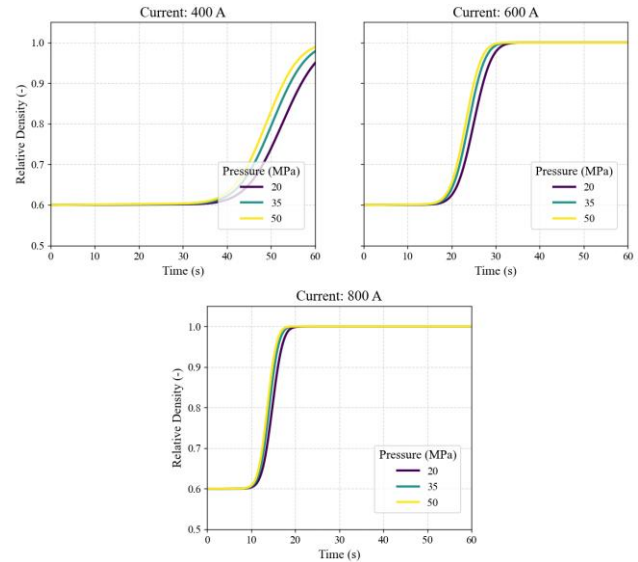


**Figure 6:** Evolution of the relative density of titanium powder during heating with current superposition

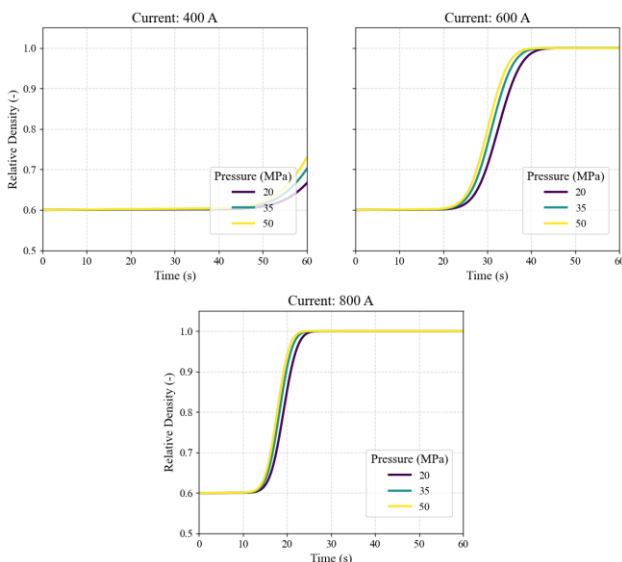


**Figure 5:** Evolution of the relative density of titanium powder during heating with pulsed current

The densification curves for current superposition (Figure 6) show a dynamics in which the consolidation process occurs almost immediately after reaching the threshold temperature. The high value of the athermal activation factor leads to a significant reduction of the material's yield limit (electroplastic effect), allowing the theoretical density (relative density > 0.995) to be achieved even under moderate external pressures. This makes this regime the most effective for producing high-density materials.

The derived "Total Energy Consumption – Final Relative Density" diagram (see Figure 7) clearly justifies the selection of the current superposition regime as the most promising. The points corresponding to this regime occupy the upper-left position on the graph, combining the highest achievable density (>0.995) with minimal total energy expenditure. These results indicate that high-quality densification can be achieved without increasing energy consumption.

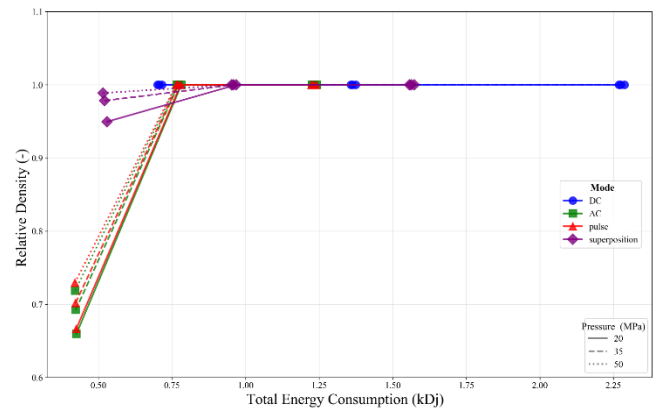


**Figure 7:** "Total Energy Consumption – Final Relative Density" diagram

For verification of the simulation results, titanium powder of PT-6 (TU U 14-10-026-98) (IT-6 TY Y 14-10-026-98) grade with an average particle diameter of approximately 60  $\mu\text{m}$  was consolidated using a superposition of direct and pulsed current at 50 kHz on the Gefest-10 system under conditions corresponding to the simulations: currents of 400, 600, and 800 A and pressing pressures of 20, 35, and 50 MPa. The temperature regime was set to reach approximately  $0.8 \cdot T_{\text{melting}} \approx 1300 \text{ }^\circ\text{C}$ , followed by holding at this temperature until  $t_{\text{max}}$ .

The temperature was monitored using a thermocouple on the surface of the die. Figure 8 shows the heating curve of the titanium powder, recalculated according to the die temperature using the heat exchange equations.

Figure 9 shows the actual densification curve obtained during the physical experiment. A comparative analysis with the simulated curve (see Figure 6) reveals an overall agreement in trends; however, the experimental curve exhibits a smoother initial stage, often referred to as the "incubation period."

This discrepancy can be attributed to several physical factors not fully accounted for in the model: the presence of oxide films on powder particle surfaces, which require time and energy for electrical breakdown; imperfect contacts between particles at the start of the process; and the thermal inertia of the tooling and

temperature sensors, which causes a delay in recording the onset of active densification.

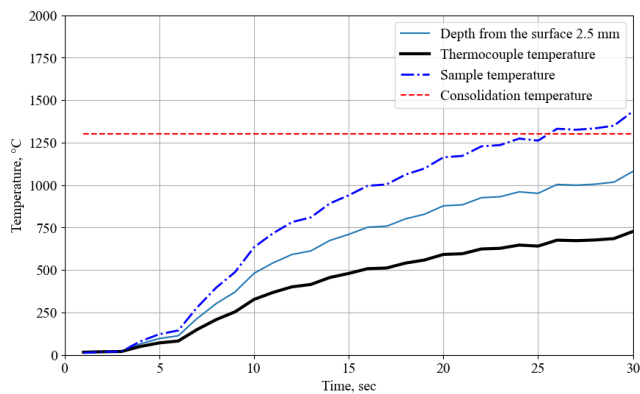


**Figure 8:** Heating curve of titanium powder under current superposition

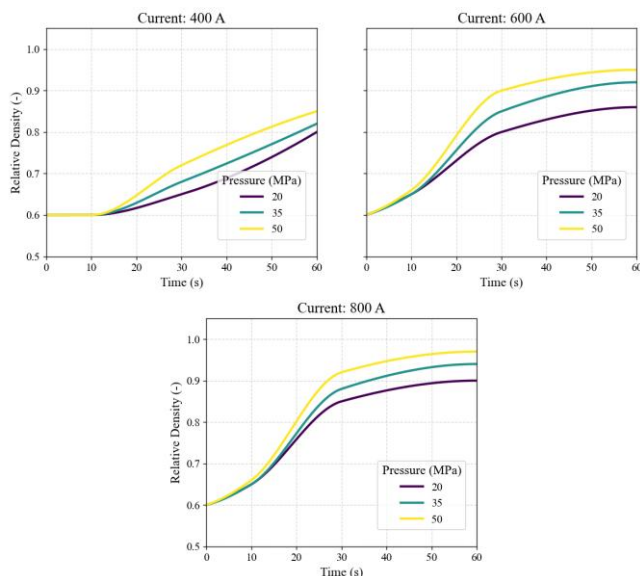


**Figure 9:** Experimental data of the specific density of titanium samples consolidated by current superposition versus consolidation time

#### 4. Conclusions

1. It has been scientifically established that consolidation under direct current exhibits classical thermal kinetics, where the densification rate is linearly dependent on temperature. This regime is stable but requires a long time (over 150 s at 400 A) to achieve high density.

2. It was found that using 50 Hz alternating current introduces a cyclic loading effect, which enhances densification during the later stages of the process. However, the lower average heating rate compared to pulsed regimes limits its effectiveness at the initial stage of consolidation.

3. It has been theoretically shown that the pulsed regime (1 kHz) likely promotes effective particle surface cleaning and accelerated neck formation due to high peak current values and the presence of pauses, enabling faster achievement of high-density materials than with direct current.

4. A scientific hypothesis was proposed and justified based on simulation results regarding the synergistic effect of combining direct and alternating current components (50 kHz). This effect manifests as the highest heating rate and the activation of the electroplastic effect, allowing the theoretical density of the material to be reached in minimal time.

5. Analysis of the “energy–density” diagrams theoretically substantiates that the current superposition regime represents the technological optimum, as it uniquely combines the maximum physico-mechanical quality of the consolidated sample (relative

density > 99.5%) with the lowest specific energy consumption, outperforming traditional methods.

6. Comparison of calculated and experimental data confirmed the adequacy of the developed model for predicting the final material properties. Observed deviations in the kinetics during the initial stage highlighted the influence of surface oxide films and contact resistances, which should be considered in further model refinements.

7. Based on the “Total Energy Consumption – Final Relative Density” analysis, the optimal titanium powder consolidation regime was identified: superposition of direct and alternating currents (50 kHz) with a total current of 600 A under a pressing pressure of 50 MPa. This regime achieves a relative density of 99.8% in less than 60 s, combining a high heating rate with intensified mass transport (characteristic of the AC component). Specific energy consumption is 15–20% lower compared to regimes achieving similar density purely via thermal effects, making this regime the most promising for industrial implementation.

#### 5. References

1. Spark Plasma Sintering Systems. Dr. Sinter Lab Series : product catalog / SPS Syntex Inc. – Kawasaki, Japan, 2023. – 12 p.
2. Field Assisted Sintering Technology (FAST) / Spark Plasma Sintering (SPS) : systems specification / FCT Systeme GmbH. – Rauenstein, Germany, 2022. – 8 p.
3. Gleeble 3800 Physical Simulation System : user guide / Dynamic Systems Inc. – Poestenkill, NY, USA, 2019. – 45 p.
4. O. Syzonenko, M. Prystash, A. Zaichenko, O. Kovalenko, Materials Science. Non-Equilibrium Phase Transformations. 4(2), 41–44 (2018).
5. Halliday, D., Resnick, R., & Walker, J. (2013). Fundamentals of Physics. 10th Edition. Wiley.
6. Olevsky, E. A. (1998). Theory of sintering: from particular models to continuum theory. Materials Science and Engineering: R: Reports, 23(2), 41-100. (У статті розглядаються різні моделі для ефективних властивостей пористих тіл).
7. Nilsson, J. W., & Riedel, S. A. (2015). Electric Circuits. 10th Edition. Pearson.
8. Incropera, F. P., DeWitt, D. P., Bergman, T. L., & Lavine, A. S. (2007). Fundamentals of Heat and Mass Transfer. 6th Edition. Wiley.
9. German, R. M. (2014). Sintering: From Empirical Observations to Scientific Principles. 2nd Edition. Butterworth-Heinemann.
10. Atkins, P., & de Paula, J. (2014). Atkins' Physical Chemistry. 10th Edition. Oxford University Press.
11. Orrù, R., Licheri, R., Locci, A. M., Cincotti, A., & Cao, G. (2009). Consolidation/synthesis of materials by electric current activated/assisted sintering. Materials Science and Engineering: R: Reports, 63(4-6), 127-287.
12. ASM Handbook, Volume 2: Properties and Selection: Nonferrous Alloys and Special-Purpose Materials. (1990). ASM International.
13. Incropera, F. P., DeWitt, D. P., Bergman, T. L., & Lavine, A. S. (2007). Fundamentals of Heat and Mass Transfer. 6th Edition. Wiley.
14. Munir, Z. A., Anselmi-Tamburini, U., & Ohyanagi, M. (2006). The effect of electric field and pressure on the synthesis and consolidation of materials: A review of the spark plasma sintering method. Journal of Materials Science, 41(3), 763–777.
15. Grasso, S., Sakka, Y., & Maizza, G. (2009). Electric current activated/assisted sintering (ECAS): a review of patents 1906–2008. Science and Technology of Advanced Materials, 10(5), 053001.

#### Acknowledgements

Authors would like to express gratitude to the Armed Forces of Ukraine for their bravery which made this work possible even in the dark times of war.